Stretch-Coil Transition and Transport of Fibers in Cellular Flows

Y.-N. Young[1] and Michael J. Shelley[2]

[1]*Department of Mathematical Sciences, New Jersey Institute of Technology, Newark, New Jersey 07102, USA*
[2]*Courant Institute of Mathematical Sciences, New York University, New York, New York 10012, USA*

(Received 8 February 2007; published 2 August 2007)

It is shown that a slender elastic fiber moving in a Stokesian fluid can be susceptible to a buckling instability—termed the ''stretch-coil'' instability—when moving in the neighborhood of a hyperbolic stagnation point of the flow. When the stagnation point is part of an extended cellular flow, it is found that immersed fibers can move as random walkers across time-independent closed-streamline flow. It is also found that the flow is segregated into transport regions around hyperbolic stagnation points and their manifolds, and closed entrapment regions around elliptic points.

DOI: 10.1103/PhysRevLett.99.058303 PACS numbers: 83.60.Wc, 47.57.eb, 87.15.Aa, 91.60.Ba

Simple shearing and straining are often used to probe the mechanical responses of deformable media [1]. For a complex fluid even such simple forcing can induce nontrivial dynamics in the fluid's microstructure. Shearing a suspension of microscopic fibers beyond a critical rate can induce fiber buckling, leading to the appearance of normal stress differences [2–4]. Straining a polymer suspension can induce coil-stretch transitions [5,6], a process recently visualized in strongly mixing elastic flows [7]. The relation between microstructural dynamics and macroscopic mechanical properties of the fluid is essential to understanding novel dynamics of elastic turbulence and mixing [8].

Buckling instabilities of fibers have also arisen as modulators of transport. Actin filaments (a biological polymer) are observed to be propelled along myosin coated surfaces [9], showing a meandering dynamics with apparent bucklings driving changes in direction. Conceived as a technique for assaying the mechanical properties of such biopolymers, it was proposed that the consequent wandering, perhaps random, motion resulted from spatial inhomogeneity of myosin density on the plate.

Inspired by such observations, we consider the dynamics and transport of elastic fibers in simple time-independent, incompressible, spatially periodic cellular flows. We focus on a 2D cellular flow (see Fig. 1 inset) where each periodic patch is a set of four vortices whose flow creates a hyperbolic stagnation point (at inset center) that is itself connected to other such stagnation points by stagnation point streamlines—its so-called stable or unstable manifolds. Such a closed-streamline cellular flow is a poor mixer as no global mixing between cells can occur in the absence of molecular diffusion. We show that an elastic fiber can be transported across such a flow as a random walker (Fig. 1), with random choices of direction induced by the internal filament dynamics in the neighborhood of hyperbolic stagnation points. This is unlike the translational diffusion due to interaction of filaments in dilute or semidilute regimes [10], or the self-diffusion of flexible filaments ([11] and references therein).

Underlying this transport is a bifurcation, complementary to the coil-stretch transition. Above a critical compressional strain rate, a straight filament (the rest state) becomes unstable to buckling at a hyperbolic stagnation point and can become folded, or ''coiled.'' This allows the fiber to sample the flow spatially, exiting along one or the other direction of the unstable manifold, and becoming stretched again as it moves to the next stagnation point.

Consider a slender, inextensible and elastic filament of radius r and length L (with $\epsilon = r/L \ll 1$), and rigidity B, moving in a Stokesian flow of viscosity μ and characteristic strain rate $\dot{\gamma}$. We neglect Brownian forces ($\sim kT/L$) relative to drag and elasticity forces ($\sim \mu\dot{\gamma}L^2$ and Yr^4/L^2, respectively; Y is the Young modulus). Predominance of drag force requires $L \gg L_1 = (kT/\mu\dot{\gamma})^{1/3}$, which for water and $\dot{\gamma} = 1\ \mathrm{s}^{-1}$ gives $L_1 \sim 1\ \mu$m. Predominance of elastic forces requires $L \gg L_2 = (kT/Y\epsilon^4)^{1/3}$, which for $\epsilon = 10^{-3}$ and $Y = 1$ GPa yields $L_2 \sim 1\ \mu$m.

The background fluid velocity field is taken to be $(W\dot{\gamma})\mathbf{U}(\mathbf{x}/W)$ where W is the cell size and $\dot{\gamma}$ is a strain rate at a hyperbolic point. Denote the fiber centerline by $\mathbf{X}(s, t)$, where s is arc length, and scale space on L, and time on $\dot{\gamma}^{-1}$. From slender-body theory [12] the leading order dynamics is governed by a local balance of drag forces with filament forces upon the fluid:

$$\eta\mathbf{D}(\mathbf{X}_t - \alpha^{-1}\mathbf{U}(\alpha\mathbf{X})) = -(\mathbf{X}_{ssss} - (\sigma(s)\mathbf{X}_s)_s) \quad (1)$$

where $\mathbf{D} = \mathbf{I} - (1/2)\mathbf{X}_s\mathbf{X}_s$ is an anisotropic drag tensor, $\alpha = L/W$ is the ratio of filament length to cell size, and $\eta \equiv 8\pi\mu\dot{\gamma}L^4/Bc$ is the effective viscosity [with $c = -\log(\epsilon^2 e)$]. Filament forces are described by Euler-Bernoulli elasticity: $\mathbf{f} = \mathbf{X}_{ssss} - (\sigma(s)\mathbf{X}_s)_s$. The line tension σ is determined by the constraint of inextensibility, expressed as $\mathbf{X}_s \cdot \mathbf{X}_{ts} = 0$, which yields a second-order boundary value problem. Zero total force and torque on the filament is satisfied by the ''free-end'' conditions $\sigma = 0$ and $\mathbf{X}_{ss} = \mathbf{X}_{sss} = \mathbf{0}$ at $s = \pm 1/2$. With our choice of scaling, α drops out of the dynamics for any linear background flow (e.g., simple strain or linear shear). This system can be posed variationally with Rayleigh dissipation function $\mathcal{D} = (\eta/2)\int ds\mathbf{X}_t\mathbf{D}\mathbf{X}_t$, and (elastic) energy, $\mathcal{E} = (1/2)\int ds\mathbf{X}_{ss}^2$ (decaying in the absence of forcing).

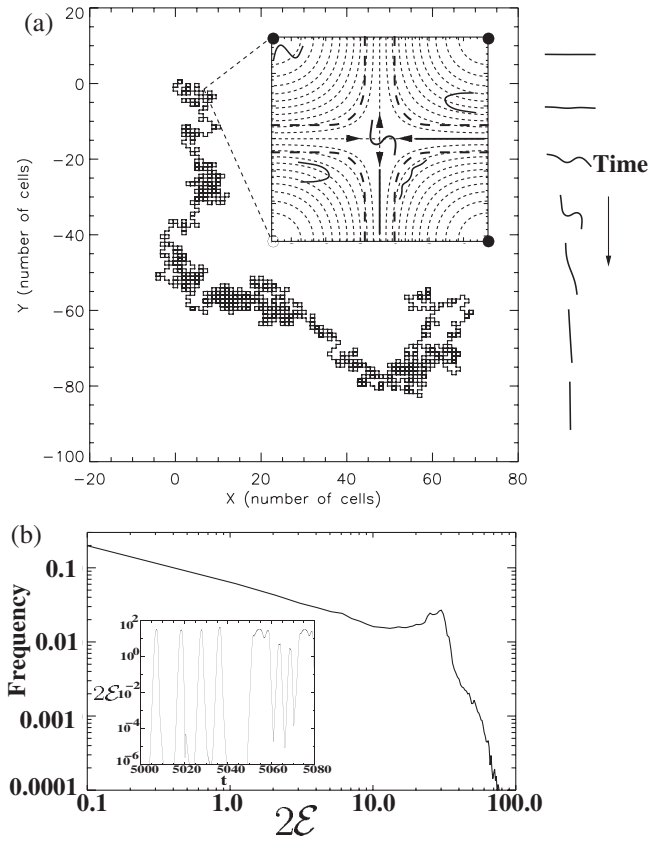

FIG. 1. (a) For $\eta = 4000$ and $\alpha = 1/\pi$, the center-of-mass trajectory of a meandering filament (box is 100×120 cells). The inset shows the streamlines (light dashed curves) of four quarter-cells of the periodic background flow, with (elliptic) vortical centers at each corner, and a hyperbolic stagnation point at the center. Also shown is a filament undergoing a stretch-coil instability as its transits through the center stagnation point (entering right, exiting down). The thick dashed curves separate regions of transport from entrapment, the dynamics of the latter shown by the filament shapes within. (b) The histogram of fiber elastic energy $2\mathcal{E}$. The inset shows a sample evolution of $2\mathcal{E}$.

The Hasimoto transformation is utilized to convert Eq. (1) to an equation for the complex curvature of the filament centerline [13]. The resultant system is numerically integrated (second-order in space and time) to simulate the filament motion in a given background flow $\mathbf{U}$.

We focus on a simple time-independent, 2D periodic flow, $\mathbf{U} = (\sin x \cos y, -\cos x \sin y, 0)$, with hyperbolic stagnation points at $(n\pi, m\pi, 0)$ for m, n integers [e.g., near $(0, 0, 0)$, $\frac{1}{\alpha}\mathbf{U}(\alpha\mathbf{x}) \approx (-x, y, 0)$]. The basic periodic structure contains four cells, or vortices, of width π, and is similar to a four-roll mill or cross-channel flow [14,15]. Hence $\alpha = L'/\pi$, with L' the relative filament length.

For $\eta = 4000$ and $\alpha = 1/\pi$, Fig. 1(a) shows the "meandering" trajectory of an initially straight filament released near a stable manifold ($x = n\pi$ or $y = m\pi$). Its dynamics is roughly this: the filament aligns with the stable manifold as it approaches a hyperbolic stagnation point. The viscous stresses of the local straining flow compress the filament along its axis, and if sufficiently high, the filament buckles. The now coiled filament samples the local velocity field around the hyperbolic point, and exits along its unstable manifold, the direction chosen with apparent randomness. The consequence is filament transport across space as a random walker.

Figure 1(b) shows the histogram of elastic energy $\mathcal{E}$ accumulated over long time. Persistent filament buckling along the meandering trajectory appears as the high curvature peak in the histogram. The temporal dynamics of $\mathcal{E}$ illustrates these transitions. Its episodic rise and fall, roughly over an order of 10 time units, corresponds to the coiling and stretching of the filament.

The rapid temporal growth in elastic energy results from a buckling instability near the stagnation point and can be analyzed, as in the shearing case [2,16]. First, an initially straight filament remains so while moving in any linear background flow. Consider then a nearly straight filament in the straining flow $(x, -y)$ (dropping the third dimension). The linearized dynamics for the perturbation amplitude z from the straight filament is $\eta(z_t - z\cos(2\theta)) = -z_{ssss} + 2\sigma_s z_s + \sigma z_{ss}$, where $\sigma(s) = \eta\cos(2\theta)/4(s^2 - 1/4)$, and $\theta(t)$ is the filament angle with the x axis. If $\theta(t)$ varies slowly, this linear equation can be taken as a homogeneous, constant coefficient partial differential equation and is amenable to standard eigenvalue analysis. A particularly simple and relevant case is $\theta = 0$, where the filament is being compressed along the stable manifold, results for which are shown in Fig. 2.

This analysis reveals that a filament can undergo a compressive buckling instability if moving towards the stagnation point in the quadrant $-\pi/4 \le \theta \le \pi/4$ around the stable manifold (Fig. 2 inset). This instability occurs at

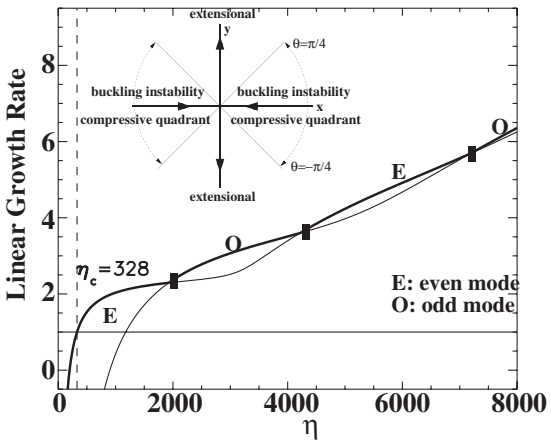

FIG. 2. Growth rate for the two dominant bending modes versus η for a filament aligned with the stable manifold ($\theta = 0$). The "E" and "O" label whether the dominant eigenfunction is even or odd about the filament center. The onset of buckling instabilities occurs for an even mode at $\eta_c \approx 328$. The inset shows the regions of compressive flow (potentially yielding a buckling instability) and extensional flow around the hyperbolic stagnation point for the straining flow $\mathbf{U} = (-x, y, 0)$.

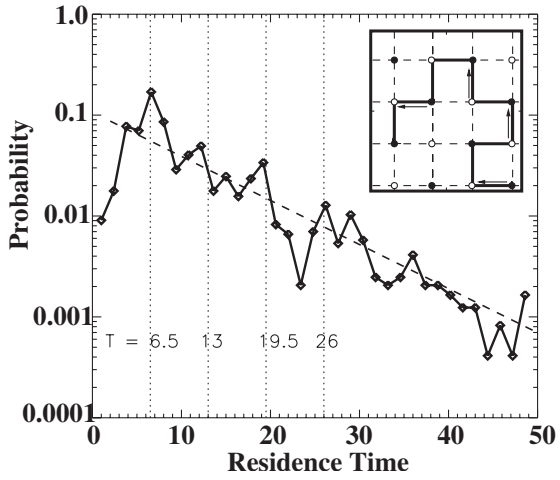

FIG. 3. Residence time frequency for $\eta = 4000$ and $\alpha = 1/\pi$. The dashed line is $P(\tau)$ with $\Delta\tau = 6.5$. The vertical lines correspond to the frequency peaks. The inset shows an idealized filament trajectory across the network of hyperbolic points.

a critical $\eta = \eta_c$; for $\eta = 4000$, as in the simulation of Fig. 1, $\eta_c \approx 328$ (for $\theta = 0$). We refer to the instability boundary as the stretch-coil transition boundary, and it is plotted (bottom dashed line) in Fig. 5.

It is this instability that drives the meandering dynamics. For this simulation Fig. 3 shows the residence time frequency, where residence time is the time a fiber moves within a particular cell. This plot is multiply peaked and shows an overall exponential decay. A very simple model of this dynamics is as a walker moving on the lattice of hyperbolic points, as illustrated in the Fig. 3 inset. If we assume that the choice of particle exit direction (up or down at open circles, left or right at closed circles) is made with equal probability of $1/2$, and is independent of the previous choice, then neglecting recurrences the discrete probability distribution for residence time τ is given by $P(\tau) = (\ln 2/\Delta\tau)(1/2)^{\tau/\Delta\tau}$, where $\tau = N\Delta\tau$ with $\Delta\tau$ the transit time between lattice points. With no *a priori* estimate available, the value of $\Delta\tau$ in the exponential distribution plotted in Fig. 3 is taken as the location of the first and highest peak of the residence time frequency. The discrete probability captures the successive peaks in the frequency plot, each corresponding to successive direction choices that keep the filament within a single cell.

Given the average transit time $\Delta\tau$, the effective filament diffusivity is $D \equiv \alpha^{-2}/4\Delta\tau$. Taking $\Delta\tau \sim 6.5$ and $\alpha = 1/\pi$ gives $D \sim 0.38$. The diffusivity can also be estimated from the fiber dispersion $d^2(t)$ [10], which for a Brownian walker satisfies $d^2 \sim 4Dt$ for large t. Figure 4 shows d^2 estimated by an ensemble average of 80 simulations for different initial filament placements (same location for the filament center but different filament angle with the x axis), for $\alpha = \pi^{-1}$ and various η. Each plot shows a roughly linear increase in time, consistent with random walk statistics. The plot for $\eta = 4000$ (curve 2) is overlaid by a

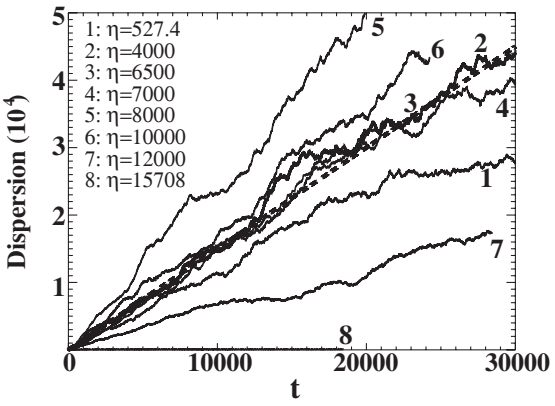

FIG. 4. Filament dispersion versus time for $\alpha = 1/\pi$ and various η, each estimated by an ensemble average of 80 simulations. The dashed line is the estimate for a random walker, $d^2(t) = 4Dt$, using the estimated diffusion $D = 0.38$ for $\eta = 4000$ (cf. curve 2).

dashed line of slope $4D$ with $D = 0.38$, showing consistency with the estimate of D found using the residence time frequency distribution. The figure also suggests that the diffusivity remains almost identical for $4000 \leq \eta \leq 7000$ (curves 2, 3, and 4), but decreases for $\eta = 527.4$ (curve 1), which is slightly above η_c, the critical value for instability. For increasing η, the implied diffusivity is nonmonotonic, increasing towards $\eta = 8000$ (curve 5), then monotonically decreasing at yet higher values (curves 6 and 7). For $\eta = 15\,708$ the filament is curved and trapped inside the cell, as shown in Fig. 5, and no diffusive transport is found.

Figure 5 depicts the numerically determined transitions in filament dynamics in the $\eta - \alpha$ plane. Note that the

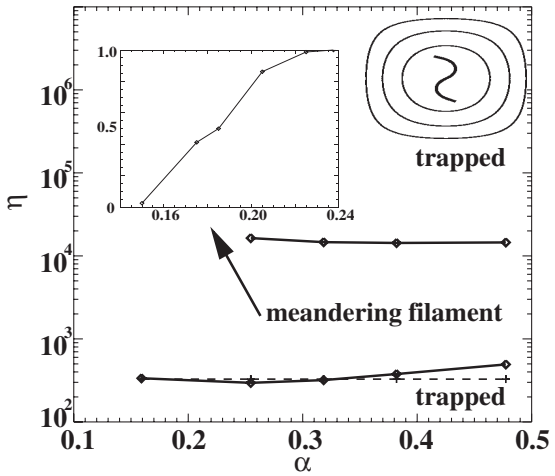

FIG. 5. Phase diagram of filament dynamics in cellular flow. For a given α, there is a range of η for meandering. The dashed line is the stretch-coil instability threshold. Inset at left shows the probability for a filament to be trapped in the cell as a function of initial distance to the manifold for $\alpha = 1/\pi$. Inset at right is for $\alpha = 1.5/\pi$ and $\eta = 80\,000$. Animations of filament dynamics can be found at [19].

lower boundary of transport (solid line) from simulations almost coincides with the stretch-coil boundary. Below this lower boundary a filament either settles to a stagnation point or stays trapped within a cell. For $\eta_c < \eta \lesssim 1.5 \times 10^4$, diffusive filament transport (meandering) is found if the filament is released not too far from the manifolds. The inset graph shows the estimated probability of a filament being trapped in the cell as a function of its initial distance to a manifold. We define the size of the transport region by the distance that corresponds to 50% for the trapping probability. For $\alpha = 1/\pi$ this distance is ~ 0.2 (i.e., the dashed curves in Fig. 1(a) inset), and seems insensitive to η. For yet larger η the region of transport collapses, and the filament is trapped in the interior as in the inset.

Finally, to seek some comparison with experimental observation, Fig. 6 shows the frequency distributions for speed of meandering filaments for various η. These distributions are bimodal, as observed in the actin transport experiments of Bourdieu *et al.* [9] at higher myosin densities. The bimodality reflects the basic dynamics underlying filament transport. The sharp peak near unity for all distributions is associated with transport between successive hyperbolic points. The secondary peak at lower velocities reflects the ''loitering'' of filaments near hyperbolic points as the buckling instability develops, and which seems to be influenced by its geometric details. For $\eta_c < \eta < 2000$ the buckling instability is dominated by an even mode (Fig. 2), and the secondary peak moves to the right as η increases in this range. For $\eta > 2000$, competition between even and odd modes leads to a more complex distribution (e.g., $\eta = 4000$), and the more prominent the odd mode the more the secondary peak moves towards lower speeds. As the even mode takes over for η above 4250, the secondary peak shifts upwards.

Here we demonstrate a flexible-fiber analog to the coil-stretch instability first predicted by de Gennes [5]. By arguing for bistability of coiled and stretched states, he also predicted that this transition was hysteretic, as was later demonstrated experimentally [17]. The important ingredients—conformation dependent drag and nonlinear elastic forces—are present here though the outcome is much more difficult to analyze. Important forces neglected here—Brownian forces and fiber-fiber hydrodynamic interactions—need to be examined for their effect on the transition we report here, as does whether complex flows can be generated by semiflexible polymers suspension (see [18] for preliminary simulations), as has been demonstrated for dilute polymer-coil suspensions.

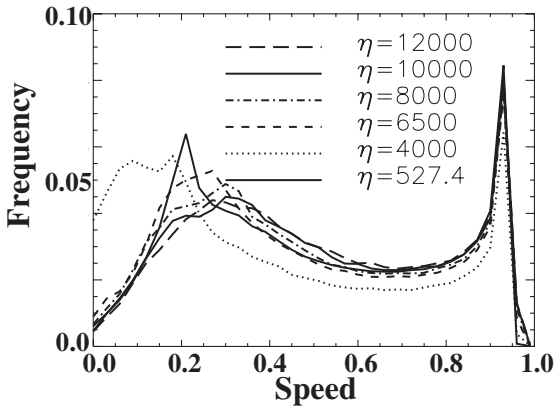

FIG. 6. The probability of filament center-of-mass speed.

We thank C. Schroeder for useful conversations, and acknowledge support from the NSF (No. DMS-0412203 and DMS-0420590), the DOE (No. DE-FG02-88ER25053), and NJIT (SBR grant).

[1] R. Larson, *The Structure and Rheology of Complex Fluids* (Oxford University Press, New York, 1998).
[2] L. E. Becker and M. J. Shelley, Phys. Rev. Lett. **87**, 198301 (2001).
[3] M. Zirnsak, D. Hur, and D. Boger, J. Non-Newtonian Fluid Mech. **54**, 153 (1994).
[4] S. Kharchenko, J. Douglas, J. Obrzut, E. Grulke, and K. Migler, Nat. Mater. **3**, 564 (2004).
[5] P. G. de Gennes, J. Chem. Phys. **60**, 5030 (1974).
[6] T. Perkins, D. Smith, and S. Chu, Science **276**, 2016 (1997).
[7] S. Geraschenko, C. Chevallard, and V. Steinberg, Europhys. Lett. **71**, 221 (2005).
[8] A. Groisman and V. Steinberg, Nature (London) **405**, 53 (2000).
[9] L. Bourdieu, T. Duke, M. B. Elowitz, D. A. Winkelmann, S. Leibler, and A. Libchaber, Phys. Rev. Lett. **75**, 176 (1995); L. Bourdieu, M. O. Magnasco, D. A. Winkelmann, and A. Libchaber, Phys. Rev. E **52**, 6573 (1995).
[10] M. Rahnama, D. L. Koch, Y. Iso, and C. Cohen, Phys. Fluids **5**, 849 (1993).
[11] Z. Bu, P. S. Russo, D. L. Tipton, and I. I. Negulescu, Macromolecules **27**, 6871 (1994).
[12] G. Batchelor, J. Fluid Mech. **44**, 419 (1970).
[13] K. Nakayama, H. Segur, and M. Wadati, Phys. Rev. Lett. **69**, 2603 (1992); R. E. Goldstein and S. A. Langer, Phys. Rev. Lett. **75**, 1094 (1995).
[14] X. Li and K. Sarkar, Phys. Rev. Lett. **95**, 256001 (2005).
[15] P. E. Arratia, C. C. Thomas, J. Diorio, and J. P. Gollub, Phys. Rev. Lett. **96**, 144502 (2006).
[16] T. Munk, O. Hallatschek, C. H. Wiggins, and E. Frey, Phys. Rev. E **74**, 041911 (2006).
[17] C. Schroeder, H. Babcock, E. Shaqfeh, and S. Chu, Science **301**, 1515 (2003).
[18] A.-K. Tornberg and M. Shelley, J. Comput. Phys. **196**, 8 (2004).
[19] See EPAPS Document No. E-PRLTAO-99-057732 for the stretch-coil transition of an elastic fiber in cellular flows. The resultant transport is illustrated for $\eta = 4000$ (ETA_4000.mov) and $\eta = 8000$ (ETA_8000.mov). For very large η the filament is trapped inside of the cell as shown in ETA_40000.mov for $\eta = 40\,000$. For more information on EPAPS, see http://www.aip.org/pubservs/epaps.html.